

Stand-Off Magnetometry with Directional Emission from Sodium Vapors

Rui Zhang^{1,2,3,4}, Emmanuel Klinger^{3,4}, Felipe Pedreros Bustos^{3,4,5}, Alexander Akulshin^{3,4,6}, Hong Guo^{1,*},
Arne Wickenbrock^{3,4} and Dmitry Budker^{3,4,7,†}

¹State Key Laboratory of Advanced Optical Communication Systems and Networks, Department of Electronics, and Center for Quantum Information Technology, Peking University, Beijing 100871, China

²Beijing Academy of Quantum Information Sciences, Beijing 100193, China

³Johannes Gutenberg-Universität Mainz, 55128 Mainz, Germany

⁴Helmholtz-Institut Mainz, GSI Helmholtzzentrum für Schwerionenforschung, 55128 Mainz, Germany

⁵Aix Marseille Univ, CNRS, CNES, LAM, Marseille 13013, France

⁶Optical Sciences Centre, Swinburne University of Technology, Melbourne 3122, Australia

⁷Department of Physics, University of California, Berkeley, California 94720, USA



(Received 7 April 2021; accepted 23 September 2021; published 21 October 2021)

Stand-off magnetometry allows measuring magnetic field at a distance, and can be employed in geophysical research, hazardous environment monitoring, and security applications. Stand-off magnetometry based on resonant scattering from atoms or molecules is often limited by the scarce amounts of detected light. The situation would be dramatically improved if the light emitted by excited atoms were to propagate towards the excitation light source in a directional manner. Here, we demonstrate that this is possible by means of mirrorless lasing. In a tabletop experiment, we detect free-precession signals of ground-state sodium spins under the influence of an external magnetic field by measuring backward-directed light. This method enables scalar magnetometry in the Earth field range, that can be extended to long-range remote sensing.

DOI: [10.1103/PhysRevLett.127.173605](https://doi.org/10.1103/PhysRevLett.127.173605)

Stand-off magnetometry [1,2], in which most of the experimental apparatus can be remote from the place where the magnetic field is measured, provides opportunity for remote geophysical research or hazardous environment monitoring. Stand-off magnetometry based on resonant scattering from atoms, in particular, laser-guide-star (LGS)-based magnetometry [2–6], where fluorescence-collection efficiency for a typical telescope is less than 10^{-10} or even lower, is often limited by the scarce number of detected photons. The problem could be solved if the excited atoms were forced to radiate towards the excitation light source in the form of laserlike emission. This is, indeed, possible using mirrorless lasing, a method to generate backward directional emission [7,8], which was demonstrated with atomic vapors confined to vapor cells [9,10]. The question of the possibility to “scale” the laboratory results to on-sky experiments remains open and is a subject of ongoing investigation [11,12].

To take advantage of directional mirrorless lasing for stand-off magnetometry, the central question is how to extract information about the magnetic field from the backward emission. It was previously observed that the threshold of mirrorless lasing and the intensity of directional radiation are sensitive to the magnetic field in the interaction region [10]. However, determining the strength of the magnetic field from the measured intensity is challenging due to the complex relation between them.

An accurate calibration and knowledge of multiple experimental parameters would be required, which is usually difficult to achieve in remote sensing schemes.

In this work, we suggest and implement mirrorless-lasing-based stand-off magnetometry, which is absolute and calibration-free, and conducted proof-of-principle laboratory experiments with a sodium vapor cell. The method is based on the principle of “free” evolution of the ground state atomic spins under the influence of the magnetic field [13]. To implement this method, we perform the measurement in three stages: (1) Optical pumping of the ground-state spin polarization; (2) Free evolution of the atomic spins “in the dark”; (3) Read out of the atomic polarization via mirrorless lasing, the intensity of which depends on the ground-state spin polarization. Mirrorless lasing requires the presence of sufficiently strong light to excite a high enough number of atoms in an elongated region. This necessarily perturbs the ground state and disrupts spin precession, which is incompatible with continuous readout of spin polarization commonly used in atomic magnetometers. To reconstruct the full evolution of spin polarization, we repeat this measurement and combine the results with different evolution times. The resulting spin-precession signal oscillating at the Larmor frequency enables scalar magnetometry. Considering the fact that such free-decay based magnetometers are among the most successful atomic sensors and that the returned emission does not require a retroreflector [14],

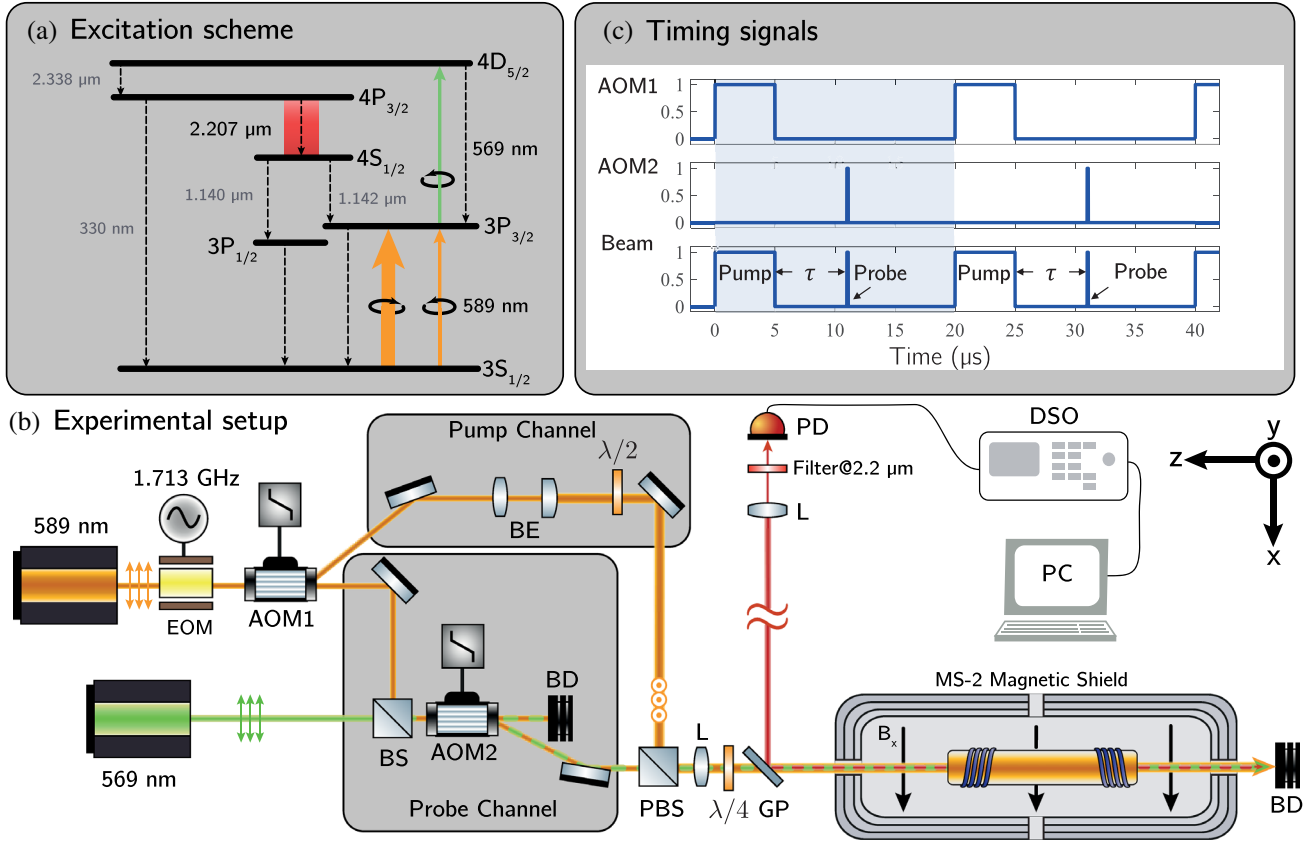


FIG. 1. Schematic of stand-off magnetometer. (a) Energy levels of sodium atoms and excitation scheme. Pump beam is a left circularly polarized 589 nm laser exciting the $3S_{1/2} \rightarrow 3P_{3/2}$ transition, which generates atomic spin polarization in the $3S_{1/2}$ state; the probe beam is a combination of right circularly polarized 589 nm and 569 nm light, which excites atoms to the $4D_{5/2}$ state and therefore produces population inversion between the $4P_{3/2}$ and $4S_{1/2}$ states, thus enabling gain for 2.21 μm spontaneous emission and mirrorless lasing. (b) Experimental setup. EOM, electro-optic modulator driven by 1.713 GHz signal to generate a sideband for hyperfine repumping; AOM1, acousto-optic modulator used to pulse the pump beam; AOM2, acousto-optic modulator used to pulse the probe beam; BE, beam expander; $\lambda/2$, half-wave plate; $\lambda/4$, quarter-wave plate; PBS, polarizing beam splitter; BS, beam splitter; BD, beam dump; L, a convex lens; GP, glass plate for reflecting the mirrorless-lasing emission; PD, photodiode placed about 1.5 m away from the center of the vapor cell; DSO, digital storage oscilloscope; PC, personal computer. (c) The timing diagram. The waveforms at the top and the middle are the control pulses of AOM1 and AOM2, respectively, and the waveform on the bottom represents the light pulses sent into the vapor cell, in which τ is the free evolution of the atomic spins “in the dark.”

our method is promising for highly sensitive, adjustment-free, long-range remote magnetometry.

The experimental arrangement is shown in Fig. 1. Light from a Coherent CR-699 dye laser at 589 nm tuned to the sodium D_2 line ($3S_{1/2} \rightarrow 3P_{3/2}$ transition), see Fig. 1(a), passes through an electro-optic modulator (EOM), see Fig. 1(b), to produce sidebands used for efficient hyperfine repumping. The beam then passes through an acousto-optic modulator (AOM1) that can switch the light power between the zeroth and first diffraction orders. The light from the first diffraction order is steered into a buffer-gas-free sodium vapor cell (3 cm diameter and 10 cm length) to generate atomic spin polarization in the ground state. The zeroth diffraction order beam is combined with the light from another dye laser (Coherent CR-899) at 569 nm tuned to the $3P_{3/2} \rightarrow 4D_{5/2}$ transition. The combined beam is passed through a second AOM (AOM2) which is used to

control the timing of optical excitation from the polarized ground state at a specific time. The probe beam excites ground-state atoms up to the $4D_{5/2}$ state enabling mirrorless lasing on population inverted transitions. Mirrorless-lasing emission at 2.21 μm is detected in the backward direction with an InGaAs photodetector (Thorlabs PDA10D2, 25 MHz bandwidth) placed 1.5 m away from the center of the vapor cell. At this distance, the 2.21 μm ($1/e^2$) beam radius is measured to be $8.87(\pm 0.23)$ mm and the divergence half-angle is estimated to be 8.1 mrad. The timing diagram is depicted in Fig. 1(c). The control pulses to AOM1 and AOM2 have the same repetition rate (50 kHz), but different duty cycle and phase. Each period starts with a pulse of 5 μs duration sent to AOM1, which generates a pump optical pulse to polarize the sodium atoms. After the end of the pump pulse, the spin polarization evolves freely. After some time, a shorter pulse is

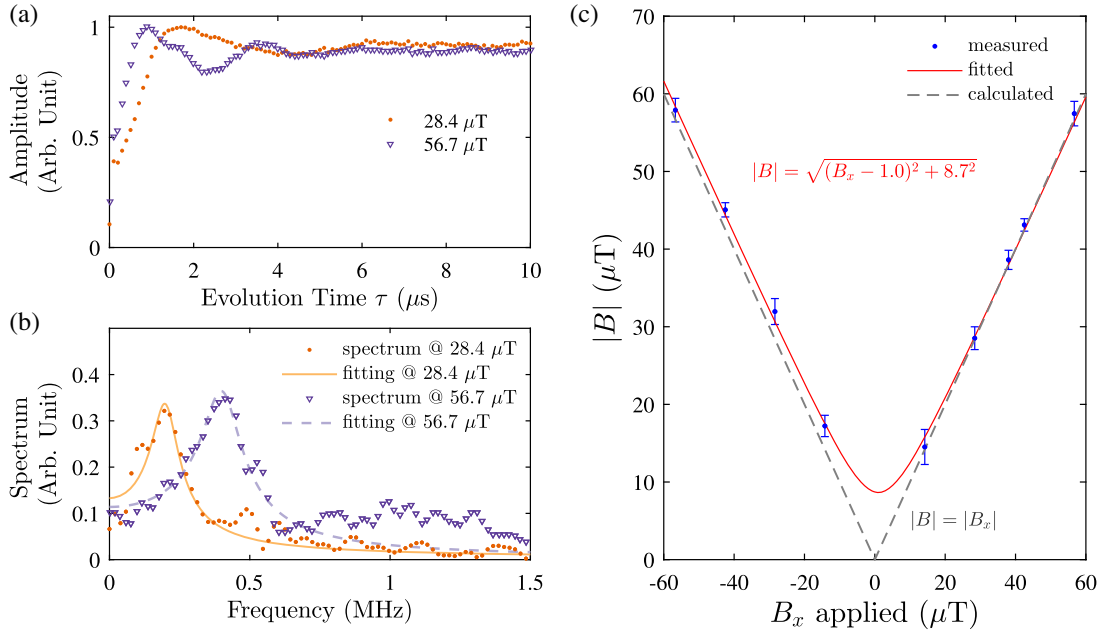


FIG. 2. (a) Orange dots (purple triangles) represent the free-precession signal with 28.4 μT (56.7 μT) bias magnetic field applied along the x direction. For each evolution time, we average readouts from 3000 modulation periods (20 μs) and the total integration time for each free-precession signal is about 6 s. (b) The amplitude spectrum of the free precession signal with 28.4 μT (56.7 μT) bias magnetic field shown in (a) and its Lorentzian fitting are represented by orange dots (purple triangles) and the light orange solid line (light purple dashed line), respectively. (c) Blue points: measured magnetic fields at different B_x applied, which are derived from the central frequencies of the Lorentzian fitting, as shown in (b); red line: a fitting of the measured magnetic fields, which suggests a $1.0(\pm 0.4)$ μT residual magnetic field along $-x$ direction and a $8.7(\pm 1.2)$ μT residual magnetic field in the y - z plane in the magnetic shield; gray dashed line: a line that assumes no residual magnetic field in the magnetic shield, so that the total magnetic strength $|B|$ equals to the applied $|B_x|$.

sent to AOM2, generating a probe-beam pulse and a subsequent mirrorless-lasing emission. As the mirrorless lasing is pulsed at the 50 kHz repetition rate, we accumulate the signal in a digital storage oscilloscope and then analyze the data to extract the pulse amplitude, which reflects the state of the spin polarization at a given evolution time. A combination of results with different evolution times represents the full revolution of the spin polarization, as shown in Fig. 2(a).

The energy levels of sodium atoms and the excitation scheme are shown in Fig. 1(a). The pump beam at 589 nm is resonant with the sodium D_2a line (from $3S_{1/2}$, $F = 2$ to $3P_{3/2}$, $F' = 1, 2, 3$). It is left circularly polarized such that it polarizes the sodium ground state spin. Probing is based on mirrorless lasing in sodium [10], in which the atoms in the $3S_{1/2}$ ground level were pumped into the $3P_{3/2}$ state with right circularly polarized 589 nm light and some of them were further pumped to the $4D_{5/2}$ state with right circularly polarized 569 nm light. Atoms in the $4D_{5/2}$ state decay into the $4P_{3/2}$ state resulting in population inversion between the $4P_{3/2}$ and $4S_{1/2}$ states. Such population inversion provides gain for the 2.21 μm spontaneous emission. As population-inverted atoms are contained in an elongated interaction region defined by the probe beam, mirrorless lasing occurs in the forward and backward directions. The

backward-directed radiation is detected with the photo-detector as shown in Fig. 1(b). It is important for our technique that the intensity of the backward emission depends on the polarization of the ground state, as these $\Delta m = 1$ transitions induced by the probe beam starting from different ground Zeeman sublevels have different transition rates and thus both the amount and polarization of excited atoms depend on the distribution of atoms among the ground Zeeman sublevels, or the ground-state polarization. The ground-state polarization dependence of mirrorless lasing can be modeled using the density-matrix (Maxwell-Bloch) approach [11] taking into account the change of the atomic and optical parameters per unit of length as a function of time.

Typical spin-evolution signals detected via mirrorless lasing, Fig. 2(a), are characterized by a damped oscillation. We change the evolution time of the spin polarization from 0 μs to 10 μs with a 0.1 μs step and record 3000 periods from the oscilloscope for each evolution time. For these measurements, we have a modulation period of 20 μs , a pump pulse width of 5 μs , and a probe pulse width of 0.4 μs . Consequently, the total integration time for each free-precession signal is about 6 s (considering the slow communication with various devices, for example, the waveform generator which drives the AOMs, the scanning

of each free-precession signal takes about 2 to 3 min in practice). The peak power of the pump beam is 173 mW, and the peak power of the 589 nm and 569 nm components of the probe beam is 48 mW and 49 mW, respectively. The repumping sideband of the 589 nm laser takes about 20% of the total power. The waist dimensions of the pump and probe beams at the center of the sodium cell are about 1.5 mm by 3 mm and 1 mm diameter, respectively. The vapor cell is heated to $\sim 169^\circ\text{C}$. The oscillating frequencies of the evolution signals are directly determined by the Larmor frequencies of the sodium ground state and the decay rates are determined by the transit time of sodium atoms across the pump beam. As shown in Fig. 2(a), each signal has the smallest amplitude close to zero evolution time. This is because the pump and probe beams are of opposite polarizations and the atoms are prepared in an unfavored state for mirrorless lasing during the pump stage [15]. Then, as the spin polarization precesses, the mirrorless lasing signals increase and reach the peaks when the polarization precesses for about π . After that, the oscillating amplitudes decay as the optically pumped atoms escape from the pump region and the averaged polarization decreases. When the evolution time increases to about 10 μs , the signals reach steady states, corresponding to no remaining polarization before detection. The amplitude spectra of these evolution signals are shown in Fig. 2(b), which peak at 0.20 MHz and 0.40 MHz, corresponding to the ground-state Larmor frequency at $\sim 28 \mu\text{T}$ and $57 \mu\text{T}$, respectively (the gyromagnetic ratio of $3S_{1/2}F = 2$ level is $\approx 7 \text{ kHz}/\mu\text{T}$). These two amplitude spectra deviate from the Lorentzian fitting for frequency higher than ~ 0.40 MHz and 0.70 MHz, respectively, which may be due to the contributions from high-order harmonics, as there may be some nonlinear dependence of the mirrorless lasing signal on the atomic polarization.

To test the magnetic-field dependence of this peak frequency, we measure the evolution signal at different magnetic fields B_x and use the peak frequency from the Lorentzian fitting to estimate the magnetic field strength, with the results shown in Fig. 2(c). According to a fitting represented by the red line, there is a $1.0(\pm 0.4) \mu\text{T}$ residual magnetic field along the $-x$ direction and a $8.7(\pm 1.2) \mu\text{T}$ residual magnetic field in the y - z plane in the magnetic shield. Such magnetic-field dependence of these peak frequencies suggests that this method could be used for magnetometry.

In conclusion, we have demonstrated scalar stand-off magnetometry based on $2.21 \mu\text{m}$ mirrorless lasing with a buffer-gas-free sodium vapor cell. With three stages of optical pumping, spin evolution in the dark, and detection via mirrorless lasing, we observed the free-precession of sodium ground-state polarization in a magnetic field. With appropriate light modulation techniques, the signal could contain also vector magnetic field information [16], which can be investigated in the future. Compared with

conventional fluorescence detection in the LGS-based magnetometry [2], the detection of backward directional emission in this work would dramatically improve the efficiency of light collection and thus the magnetometry sensitivity. Vapor cells filled with buffer gas such as He, N_2 , or Ne are expected to exhibit much longer coherence times as the atoms would spend more time in the light-beam area, which is beneficial to high-sensitivity magnetometry. Vapor-cell based stand-off magnetometers can be operated in harsh environments, for example, near nuclear reactors or particle accelerators, where it is impossible to place conventional sensors or electronics. In natural environment, e.g., near space, where atomic density is beyond control, it may be below the amplification threshold, precluding the use of the present mirrorless-lasing scheme. In this case, other schemes may be possible, for example, those with light of longer wavelength and thus potentially larger coupling cross section [11], or with other atoms or molecules of larger abundance, e.g., oxygen or nitrogen [12]. A requirement is that mirrorless lasing should depend on atomic or molecular spins. Ongoing work is exploring the feasibility of such schemes for remote geophysical magnetometry [2,6].

The authors are grateful to Aram Papoyan for helpful discussions, as well as to the European Southern Observatory for the loan of a dye-laser system. This work was supported in part by the DFG Project ID 390831469: EXC 2118 (PRISMA + Cluster of Excellence), the European Research Council (ERC) under the European Union Horizon 2020 Research and Innovation Program (Grant Agreement No. 695405), the DFG Reinhart Koselleck Project and the German Federal Ministry of Education and Research (BMBF) within the Quantumtechnologien program (FKZ 13N15064). R. Z. acknowledges support from the China Scholarship Council (CSC) enabling his research at the Helmholtz-Institut Mainz. F. P. B. received support from the European Union's Horizon 2020 research and innovation programme under the Marie Skłodowska-Curie Grant Agreement No. 893150.

*hongguo@pku.edu.cn

†budker@uni-mainz.de

- [1] J. P. Davis, M. B. Rankin, L. C. Bobb, C. Giranda, and M. J. Squicciarini, *REMAS Source Book*, Mission and Avionics Tech. Dept., Naval Air Development Center, 1989.
- [2] F. Pedreros Bustos, D. Bonaccini Calia, D. Budker, M. Centrone, J. Hellemeier, P. Hickson, R. Holzlöhner, and S. Rochester, Remote sensing of geomagnetic fields and atomic collisions in the mesosphere, *Nat. Commun.* **9**, 3981 (2018).
- [3] J. M. Higbie, S. M. Rochester, B. Patton, R. Holzlöhner, D. Bonaccini Calia, and D. Budker, Magnetometry with mesospheric sodium, *Proc. Natl. Acad. Sci. U.S.A.* **108**, 3522 (2011).

- [4] T. J. Kane, P. D. Hillman, C. A. Denman, M. Hart, R. P. Scott, M. E. Purucker, and S. J. Potashnik, Laser remote magnetometry using mesospheric sodium, *J. Geophys. Res.* **123**, 6171 (2018).
- [5] T. Fan, X. Yang, J. Dong, L. Zhang, S. Cui, J. Qian, R. Dong, K. Deng, T. Zhou, K. Wei, Y. Feng, and W. Chen, Remote magnetometry with mesospheric sodium based on gated photon counting, *J. Geophys. Res.* **124**, 7505 (2019).
- [6] F. Pedreros Bustos, D. Bonaccini Calia, D. Budker, M. Centrone, J. Hellemeier, P. Hickson, R. Holzlöhner, and S. Rochester, Polarization-driven spin precession of mesospheric sodium atoms, *Opt. Lett.* **43**, 5825 (2018).
- [7] A. Dogariu, J. B. Michael, M. O. Scully, and R. B. Miles, High-gain backward lasing in air, *Science* **331**, 442 (2011).
- [8] G. O. Ariunbold, V. A. Sautenkov, Y. V. Rostovtsev, and M. O. Scully, Ultrafast laser control of backward superfluorescence towards standoff sensing, *Appl. Phys. Lett.* **104**, 021114 (2014).
- [9] J. V. Thompson, C. W. Ballmann, H. Cai, Z. Yi, Y. V. Rostovtsev, A. V. Sokolov, P. Hemmer, A. M. Zheltikov, G. O. Ariunbold, and M. O. Scully, Pulsed cooperative backward emissions from non-degenerate atomic transitions in sodium, *New J. Phys.* **16**, 103017 (2014).
- [10] A. Akulshin, F. Pedreros Bustos, and D. Budker, Continuous-wave mirrorless lasing at $2.21\ \mu\text{m}$ in sodium vapors, *Opt. Lett.* **43**, 5279 (2018).
- [11] F. Pedreros Bustos, A. Akulshin, R. Holzlöhner, S. Rochester, and D. Budker, Studies towards a directional polychromatic sodium laser guide star, *Proc. SPIE* **10703**, 107030R (2018).
- [12] P. Hickson, J. Hellemeier, and R. Yang, Can amplified spontaneous emission produce intense laser guide stars for adaptive optics?, *Opt. Lett.* **46**, 1792 (2021).
- [13] D. Budker and M. Romalis, Optical magnetometry, *Nat. Phys.* **3**, 227 (2007).
- [14] B. Patton, O. Versolato, D. C. Hovde, E. Corsini, J. M. Higbie, and D. Budker, A remotely interrogated all-optical ^{87}Rb magnetometer, *Appl. Phys. Lett.* **101**, 083502 (2012).
- [15] The delay time between the mirrorless lasing and the probe pulse is correlated with the signal amplitude and is on the order of $0.1\ \mu\text{s}$, which is much smaller than the Larmor period.
- [16] B. Patton, E. Zhivun, D. C. Hovde, and D. Budker, All-Optical Vector Atomic Magnetometer, *Phys. Rev. Lett.* **113**, 013001 (2014).